

A JWST project on 47 Tucanae. Binaries among multiple populations.

A. P. Milone^{1,2}, A. F. Marino², M. Bernizzoni¹, F. Muratore¹, M. V. Legnardi¹, M. Barbieri¹, E. Bortolan¹, A. Bouras¹, J. Bruce³, G. Cordini⁴, F. D'Antona⁵, F. Dell'Agli⁵, E. Dondoglio², I. M. Grimaldi¹, S. Jang⁶, E. P. Lagioia⁷, J.-W. Lee⁸, S. Lionetto¹, A. Mohandasan¹, X. Pang^{9,10}, C. Pianta¹, M. Posenato¹, A. Renzini², M. Tailo², C. Ventura⁵, P. Ventura⁵, E. Vesperini³, T. Ziliotti¹,

¹ Dipartimento di Fisica e Astronomia “Galileo Galilei”, Univ. di Padova, Vicolo dell’Osservatorio 3, Padova, IT-35122
e-mail: antonino.milone@unipd.it

² Istituto Nazionale di Astrofisica - Osservatorio Astronomico di Padova, Vicolo dell’Osservatorio 5, Padova, IT-35122

³ Department of Astronomy, Indiana University, Bloomington, Swain West, 727 E. 3rd Street, IN 47405, USA

⁴ Research School of Astronomy and Astrophysics, Australian National University, Canberra, ACT 2611, Australia

⁵ Istituto Nazionale di Astrofisica, Osservatorio Astronomico di Roma, Via Frascati 33, 00077 Monte Porzio Catone, Italy

⁶ Center for Galaxy Evolution Research and Department of Astronomy, Yonsei University, Seoul 03722, Korea

⁷ South-Western Institute for Astronomy Research, Yunnan University, Kunming, 650500 P. R. China

⁸ Department of Physics and Astronomy, Sejong University, 209 Neungdong-ro, Gwangjin-Gu, Seoul 05006, Republic of Korea

⁹ Department of Physics, Xi'an Jiaotong-Liverpool University, 111 Ren'ai Road, Dushu Lake Science and Education Innovation District, Suzhou 215123, Jiangsu Province, People's Republic of China

¹⁰ Shanghai Key Laboratory for Astrophysics, Shanghai Normal University, 100 Guilin Road, Shanghai 200234, People's Republic of China

Received XXXX; accepted XXXX

ABSTRACT

Almost all globular clusters (GCs) contain multiple stellar populations consisting of stars with varying helium and light-element abundances. These populations include first-population stars, which exhibit similar chemical compositions to halo-field stars with comparable [Fe/H], and second-population stars, characterized by enhanced helium and nitrogen abundances along with reduced levels of oxygen and carbon. Nowadays, one of the most intriguing open questions about GCs pertains to the formation and evolution of their multiple populations.

Recent works based on N-body simulations of GCs show that the fractions and characteristics of binary stars can serve as dynamic indicators of the formation period of multiple-population in GCs and their subsequent dynamical evolution. Nevertheless, the incidence of binaries among multiple populations is still poorly studied. Moreover, the few available observational studies are focused only on the bright stars of a few GCs.

In this work, we use deep images of the GC 47 Tucanae collected with the James Webb and the Hubble space telescopes to investigate the incidence of binaries among multiple populations of M-dwarfs and bright main-sequence stars. To reach this objective, we use UV, optical, and near infrared filters to construct photometric diagrams that allow us to disentangle binary systems and multiple populations. Moreover, we compared these observations with a large sample of simulated binaries.

In the cluster central regions, the incidence of binaries among first-population stars is only slightly higher than that of second-population stars. In contrast, in the external regions, the majority ($\gtrsim 85\%$) of the studied binaries are composed of first population stars. Results are consistent with the GC formation scenarios where the second-population stars originate in the cluster's central region, forming a compact and dense stellar group within a more extended system of first-population stars.

Key words. techniques: photometric - Hertzsprung-Russell and C-M diagrams - stars: abundances - stars: Population II - globular clusters: individual (NGC 104)

arXiv:2503.19214v1 [astro-ph.SR] 24 Mar 2025

1. Introduction

Galactic globular clusters (GCs) are among the most-ancient stellar systems in the Universe and serve as laboratories for testing theories of stellar structure and evolution. Their investigation is complementary to studies based on high redshift galaxies to shed light on the assembly of large scale structures such as the Galactic halo (e.g. Renzini 2017; D'Antona et al. 2023). One of the most fascinating properties of GCs is that a large fraction of their stars exhibits distinctive chemical compositions that are rarely observed among field stars. These 'second-population' (2P) stars are enhanced in some light elements, (including helium, nitrogen,

aluminum, and sodium) and depleted in others (e.g. carbon and oxygen) with respect to the remaining GC stars, which are indicated as 'first population' (1P) and share the same content of light elements as α -enhanced field stars with similar metallicity (see Kraft 1994; Gratton et al. 2004, 2012, 2019; Bastian & Lardo 2018; Milone & Marino 2022, for reviews).

Although the origin of multiple populations in GCs is a widely debated topic (Cottrell & Da Costa 1981; Dantona et al. 1983; D'Antona et al. 2016; Ventura et al. 2001; Decressin et al. 2007; de Mink et al. 2009; Bastian et al. 2013; Denissenkov & Hartwick 2014; Renzini et al. 2015, 2022; Gieles et al. 2018; Calura et al. 2019; Wang et al. 2020; Lacchin et al. 2022, 2024), most forma-

tion scenarios suggest that 2P stars formed in a high-density environment, in the innermost GC regions. The binary stars among the distinct stellar populations in GCs are efficient tools to test this hypothesis and constrain the cluster formation and dynamical evolution. Indeed, as a consequence of the denser formation environment, the 2P binaries should be more strongly affected by stellar interactions and disrupted at larger rates than 1P binaries (Vesperini et al. 2011; Hong et al. 2015, 2016; Hypki et al. 2022). N-body simulations by Vesperini, Hong, and collaborators show that in multiple-population clusters, a denser 2P system embedded in a less concentrated 1P cluster can lead to similar binary fractions for 1P and 2P stars in the central regions, with 1P binaries making up the majority of the total binaries (Hong et al. 2015, 2016; Milone et al. 2020; Bortolan et al. 2025).

Early observational constraints on the incidence of binaries among 1P and 2P stars of GCs rely on spectroscopy. D’Orazi et al. (2010) detected five Barium-rich stars in five GCs and noticed that four of them have content of sodium and oxygen consistent with 1P stars, whereas one star alone belongs to the 2P. The large barium abundance observed in these Ba-stars is linked to unseen evolved companions that transferred processed material to the visible star during their asymptotic giant branch phase (e.g., McClure 1989; Luck & Bond 1991). Consequently, the findings by D’Orazi and collaborators suggest a prevalence of binaries among 1P stars.

Similar conclusions come from works based on spectroscopy of binary stars identified by means of radial-velocity variations. Based on a study involving 21 radial-velocity binaries across ten GCs, Lucatello et al. (2015) concluded that the fraction of binaries among 1P stars is 4.1 ± 1.7 times higher than the fraction observed among 2P stars. This conclusion aligns with the research by Dalessandro et al. (2018), who determined that out of 12 radial-velocity binaries in NGC 6362, only one belongs to the 2P.

Most of the stars studied spectroscopically are red giant branch (RGB) stars located in the external cluster regions. The first photometric investigation of binaries in the cluster centers relies on multi-band images of bright main-sequence (MS) stars obtained with the *Hubble* Space Telescope (*HST*) and yields puzzling conclusions. In the core of M 4, the 1P binaries incidence is about three times higher than the 2P incidence (Milone et al. 2020) and a predominance of 1P binaries is also detected in the central region of NGC 3201 (Marino et al. 2019; Kamann et al. 2020). In contrast, NGC 288, NGC 6352, NGC 6362, NGC 6397 and NGC 6838 exhibit similar binary incidence rates in their central $\sim 2.7 \times 2.7$ square-arcmin regions (Milone et al. 2020, 2025).

Recently, we initiated a project to explore faint stars in the GC 47 Tucanae, by using spectra and images obtained through the *James Webb* Space Telescope (*JWST*) as part of the GO-2560 program (PI: Anna F. Marino) together with archive HST and JWST images. The initial findings from this project include the pioneering detection of the brown-dwarf cooling sequence within a GC (Marino et al. 2024a), the identification of multiple stellar populations among M-dwarfs, and the first determination of their oxygen abundances by means of both photometry and spectroscopy (Milone et al. 2023b; Marino et al. 2024a,b).

In this work, we study the incidence of binaries among 1P and 2P stars of 47 Tucanae, which is a GC that hosts a small fraction of binaries that correspond to $\sim 1\%$ in the central regions (Milone et al. 2012a). The paper is organized as follows. Section 2 presents the dataset and summarizes the data reduction techniques. Section 3 illustrates the methods to study the binaries among the multiple populations of 47 Tucanae. The distribution of binaries in the pseudo two-color diagrams dubbed ‘chromosome maps’

(ChMs) is discussed in the Section 4, whereas the Section 5 is dedicated to the summary of the results and the conclusions.

2. Observations and data reduction

To investigate the binaries among the multiple populations of 47 Tucanae, we analyzed stars in two different fields of view: a central field ($\text{RA} \sim 00^{\text{h}}24^{\text{m}}06^{\text{s}}$, $\text{DEC} \sim -72^{\text{d}}04^{\text{m}}53^{\text{s}}$) and an external field ($\text{RA} \sim 00^{\text{h}}24^{\text{m}}37^{\text{s}}$, $\text{DEC} \sim -72^{\text{d}}04^{\text{m}}06^{\text{s}}$) located at ~ 7 arcmin west of the cluster center (about $2.2 R_{\text{hl}}$ where $R_{\text{hl}} = 3.17$ arcmin is the cluster half-light radius from the 2010 version of the Harris (1996) catalogue).

We used images of the central field collected through the F435W, F606W and F814W filters of the Wide Field Channel of the Advanced Camera for Surveys (WFC/ACS) and images in the F275W, F343N, F336W, and F438W bands of the Ultraviolet and Visual Channel of the Wide Field Camera 3 (UVIS/WFC3) on board the *HST*.

For the external field, we investigated the M-dwarfs of 47 Tucanae by using the photometric catalogs by Marino et al. (2024a), which are obtained from ACS/WFC data in the F606W and F814W bands and images collected through the F322W2 filter of the near-infrared camera (NIRCam) onboard the *JWST*. In addition, we used images collected with the F336W of UVIS/WFC3 and the F435W of WFC/ACS. These data, together with the photometry in the F606W and F814W bands from Marino et al. (2024a) allowed us to explore the upper MS of 47 Tucanae. The main properties of the images used to derive the photometry used in this paper are summarized in Table 1.

Stellar photometry and astrometry are obtained using the computer program KS2, developed by Jay Anderson as an evolution of the program initially developed to reduce ACS/WFC images from GO-10775 in the F606W and F814W bands (Anderson et al. 2008). In summary, KS2 employs three methods to measure stars, optimizing astrometry and photometry for stars in different luminosity intervals. As our focus lies on relatively bright stars, we relied on the results obtained from method I. This method measures all stellar sources that produce a distinct peak within a 5×5 pixel region after subtracting neighboring stars.

To achieve this, KS2 calculates the flux and position of each star in each image separately by using the point spread function (PSF) model associated with its position. It also subtracts the sky level, which is computed from the annulus between 4 and 8 pixels from the stellar center. Finally, the results from all images are averaged to obtain the most accurate determinations of stellar magnitudes and positions. The KS2 computer program offers multiple diagnostics for assessing photometric quality. To ensure high-precision photometry, we included only isolated stars that are well-fitted by the PSF model in our analysis (see section 2.4 of Milone et al. 2023a, for details). Moreover, we excluded the region with a radial distance of less than 0.77 arcminutes from the analysis of MS stars in order to avoid the most crowded inner area. The stellar positions derived from the ACS/WFC and UVIS/WFC3 images are corrected for distortion by using the solutions provided by Anderson & King (2006), Bellini & Bedin (2009), and Bellini et al. (2011). The photometry has been calibrated into the Vega-mag system by using the procedure outlined by Milone et al. (2023a) and by adopting the encircled energy and the zero points available at the STScI web page¹.

¹ <https://www.stsci.edu/hst/instrumentation/acs/data-analysis/zeropoints>;
<https://www.stsci.edu/hst/instrumentation/wfc3/data-analysis/photometric-calibration>

We exploited stellar proper motions to separate field stars from cluster members. We calculate the proper motions of stars in the central field as in [Milone et al. \(2023a\)](#), by comparing the stellar positions of images collected at different epochs. For the external field, we used the proper motions by [Marino et al. \(2024a\)](#).

2.1. Artificial star tests

To estimate the photometric errors and create the simulated color-magnitude diagram (CMD), we conducted artificial star (AS) tests for each field. Following the method outlined by [Anderson et al. \(2008\)](#), we generated a list of 10^6 ASs with radial distributions and luminosity functions matching those of the observed stars. We adopted for the ASs the F814W instrumental magnitudes that range from the saturation limit to -5.0 mag². The photometry and astrometry of the ASs and the selection of the relatively isolated ASs that are well fitted by the PSF model have been carried out with the same procedure used for real stars.

3. Binaries among multiple populations

In this section, we describe the procedure that we used to derive the fraction of binaries among 1P and 2P stars of 47 Tucanae and present the results. In a nutshell, this method, detailed in the following subsections, is based on [Milone et al. \(2020\)](#) and [Muratore et al. \(2024\)](#) who estimated the binary incidence among multiple populations in Galactic GCs and Magellanic Cloud young star clusters. It utilizes two photometric diagrams: a CMD, where 1P and 2P stars appear indistinguishable and are used to identify binaries, and another diagram where 1P and 2P stars form distinct sequences. Binary fractions for 1P and 2P stars are inferred by comparing the color distributions of observed binaries with those from simulated CMDs containing varying 1P and 2P binary fractions. We separately analyzed stars with different luminosities and radial distances from the cluster center. Section 3.1 is focused on binaries among M-dwarfs in the external field³, whereas Section 3.2 is dedicated to the investigation of upper-MS stars in the central field.

3.1. The M-dwarfs

To estimate the fraction of binaries among the multiple populations of M-dwarfs in 47 Tucanae, we used the method illustrated in Figures 3–4, which is based on the procedure introduced by [Milone et al. \(2020\)](#) to derive the fractions of binaries composed of 1P and 2P stars along the upper MS of GCs.

The first step consists in selecting groups of bona-fide 1P and 2P stars. To do this, we used the $\Delta_{CF606W,F814W,F322W2}$ vs. $\Delta_{F606W,F814W}$ ChM of M-dwarfs introduced by [Marino et al. \(2024a\)](#), which is reproduced in the top-left panel of Figure 1. This ChM is composed of MS stars with $20.0 < m_{F814W} < 24.0$ mag, thus including the MS region where the sequences of 1P

¹ <https://jwst-docs.stsci.edu/jwst-near-infrared-camera/nircam-performance/nircam-absolute-flux-calibration-and-zero-points>

² Instrumental magnitudes are defined as the $-2.5 \log_{10}$ of the detected photo-electrons.

³ While NIRCam data are unavailable for the cluster center, the *HST* archive includes IR/WFC images in F110W and F160W (GO-11664, PI, Brown). These filters can identify multiple populations below the MS knee, but crowding makes distinguishing 1P and 2P stars in the cluster center challenging. Hence, we only investigate binaries among M-dwarfs in the external regions.

and 2P stars are more evident. As discussed by Marino and collaborators, 1P stars populate the ChM region near the origin of the reference frame, whereas the 2P defines a narrow sequence of stars that extend towards the top-left corner of the ChM. The distribution of stars along the 2P sequence is not uniform but shows stellar overdensities that correspond to sub-populations of stars with different oxygen abundances ([Marino et al. 2024a,b](#)). We identified a sample of bona-fide 1P stars, which are colored crimson in the ChM plotted in the bottom-left panel of Figure 1, and four main groups of 2P stars, which we indicated as 2P_A, 2P_B, 2P_C, and 2P_D, and colored orange, aqua, cyan, and blue, respectively.

Then, we used two pseudo-CMDs, where the multiple populations exhibit very different behaviours. In the m_{F814W} vs. $C_{F606W,F814W,F322W2}$ diagram plotted in the right panel of Figure 1 the five stellar populations identified in the ChM define distinct sequences. The pseudo-color separation among the sequences is well illustrated in the inset, where we superimposed their fiducials (continuous lines) and the corresponding fiducials of equal-luminosity binaries⁴ (dotted lines) on the pseudo-CMD. Furthermore, we introduced the m_{F814W} vs. $(m_{F606W} - m_{F160W}) - 0.55(m_{F606W} - m_{F814W})$ pseudo-CMD plotted in Figure 2, where the fiducial lines of the five selected stellar groups are nearly superimposed on each other.

The latter diagram is used to select a sample of binary systems composed of stars with similar luminosities as illustrated in Figure 3a. The 44 selected binaries are represented with large magenta triangles and are located within the yellow-shaded portion of the pseudo-CMD and delimited by the two orange fiducial lines. Specifically, the left boundary is the fiducial line composed of MS-MS binaries where the secondary component is 1.6 mag fainter than the primary star in the F814W band. Based on diagrams constructed with ASs, this adopted value allows us to minimize the contamination of single stars with large observational errors. The right boundary is the fiducial line of equal-luminosity binaries shifted to the red by three times the pseudo-color observational error. Figure 3b highlights the selected binaries in the m_{F814W} vs. $C_{F606W,F814W,F322W2}$ pseudo-CMD together with the fiducial lines of 1P and 2P_D stars (red and blue continuous lines) and the fiducial line of equal-luminosity 1P binaries (red-dotted line). These three fiducials are used to derive the verticalized m_{F814W} vs. $\delta_{CF606W,F814W,F322W2}$ plotted in panel c of Figure 3, which is obtained by using the procedure by [Milone et al. \(2017\)](#), see their Appendix A).

In a nutshell, we considered two groups of stars in the m_{F814W} vs. $C_{F606W,F814W,F322W2}$ pseudo-CMD, namely group I and II, which are located on the left and right side of the 1P fiducial line, respectively. We defined

$$\delta_{CF606W,F814W,F322W2} = \begin{cases} W_I \frac{X - X_{\text{fiducial A}}}{X_{\text{fiducial B}} - X_{\text{fiducial A}}}, & \text{for group I,} \\ W_{II} \frac{X - X_{\text{fiducial B}}}{X_{\text{fiducial C}} - X_{\text{fiducial B}}}, & \text{for group II.} \end{cases} \quad (1)$$

where $X = C_{F606W,F814W,F322W2}$. We have assumed for fiducial A, B, and C, the continuous blue, continuous red, and dotted-red fiducial lines of Figure 3b, respectively. The constant W_I and W_{II} indicates the $\Delta_{CF606W,F814W,F322W2}$ pseudo-color distance between the fiducials B and A at $m_{F814W} = 22.25$ mag. Similarly, the con-

⁴ The fiducial line for binary systems, consisting of pairs of stars with identical magnitudes, aligns with the fiducial line of the corresponding single stars but is shifted brighter by ~ 0.753 magnitudes.

Filter	Instrument	N × Exp. time	date	Program
Central field				
F275W	UVIS/WFC3	2×323s+12×348s	Nov 21 2011	12311
F336W	UVIS/WFC3	30s+2×580s	Sep 28-29 2010	11729
F343N	UVIS/WFC3	730s+1325s	Mar 23 2018	15061
F435W	ACS/WFC	10s+6×100s+3×115s	Sep 30 - Oct 11 2002	9281
F438W	UVIS/WFC3	40s+130s+435s	Mar 23 2018	15061
F606W	ACS/WFC	3s+4×50s	Mar 13 2006	10775
F814W	ACS/WFC	3s+4×50s	Mar 13 2006	10775
External Field				
F336W	UVIS/WFC3	2×300s	Sep 4 2015 - Mar 11 2016	14021
F435W	ACS/WFC	36×30s	Apr 17 2002 - May 06 2006	9018
F435W	ACS/WFC	12×350s	Sep 2 2006	10730
F435W	ACS/WFC	6×339s	Nov 27-28 2005	10730
F814W	ACS/WFC	2×1390s+2×1460s	Oct 9 2002	9444
F606W	ACS/WFC	4×1s+4×10s+4×100s+117×1113s-1498s	Jan 15 2010 - Oct 1 2010	11677
F814W	ACS/WFC	4×1s+4×10s+4×100s+125×1031s-1484s	Jan 15 2010 - Oct 1 2010	11677
F160W	IR/WFC3	24×274s	Jul 23 2009	11445
F160W	IR/WFC3	18×274s	Jul 23 2009	11453
F160W	IR/WFC3	24×92s+24×352s	Mar 3 2010 - Nov 20 2010	11931
F160W	IR/WFC3	14×92s+6×352s	Apr 9 2011 - Sep 18 2011	12352
F160W	IR/WFC3	14×92s+6×352s	Feb 14 2012 - Aug 22 2012	12696
F160W	IR/WFC3	5×92s+2×352s	Apr 19 2013	13079
F160W	IR/WFC3	5×92s+2×352s	Dec 21 2013	13563
F322W2	NIRCam	48×857s	Sep 14-15 2022	2560

Table 1. Summary of the properties of the *HST* and *JWST* used in this work.

stant W_{II} refers to the distance between the fiducials C and B at the same F814W magnitude level.

We derived the cumulative distribution of $\delta_{CF606W,F814W,F322W2}$ and the corresponding kernel-density distribution, plotted in panels d and e of Figure 3, respectively. The latter is obtained by assuming a Gaussian kernel with dispersion of 0.02 mag.

The fraction of binaries composed of two 1P stars, two 2P stars, or a 1P and 2P star (hereafter 1P, 2P, and mixed binaries) is derived by comparing the $\delta_{CF606W,F814W,F322W2}$ cumulative distribution of the observed binaries and the cumulative distributions derived from grids of simulated CMDs that are constructed by using the ASs. We assumed grids of values that range from 0% to 100% in steps of 1% for the fractions of 1P binaries (f_{bin}^{1P}), 2P_X binaries (f_{bin}^{2PX} , where X=A,B,C, and D) and the fraction of mixed binaries (f_{bin}^{MIX}). For simplicity, we assumed that the 2P components of the mixed binaries have the same probability of belonging to each of the four populations 2P_{A--D}, based on the relative fractions of stars in each of them calculated by [Marino et al. \(2024a\)](#). For each combination of f_{bin}^{1P} , f_{bin}^{2PX} , and f_{bin}^{MIX} , we derived the $\delta_{CF606W,F814W,F322W2}$ cumulative distribution of the simulated binaries by using the same photometric diagrams and the same procedure adopted for the real stars. This quantity is compared with the corresponding cumulative distribution of the observed binaries by means of χ^2 .

As summarized in Table 2, we find a predominance of 1P binaries, with the fractions of 1P and 2P binaries corresponding to $84.8 \pm 5.0\%$, and $8.2 \pm 4.5\%$ respectively. The inferred fraction of mixed binaries is $7.0 \pm 4.5\%$. The simulated diagrams that provide the best match with the observations are illustrated in the panels a and b of Figure 4, where we used aqua and black symbols to mark the simulated binary systems. The simulated cumulative and kernel-density distributions of the studied simulated binaries (aqua triangles in Figure 4a,b) are represented with aqua lines

in the panels c and d, respectively, and are compared with the corresponding observed distributions that we colored magenta.

To assess the uncertainties associated with the binary-fractions, we used ASs to create 10,000 pairs of mock m_{F814W} vs. $(m_{F606W} - m_{F160W}) - 0.55$ ($m_{F606W} - m_{F814W}$) and m_{F814W} vs. $C_{F275W,F343N,F438W}$ photometric diagrams. These diagrams were generated with identical fractions of 1P, 2P and mixed binaries as determined from the observational data. We applied the identical methodology used for real stars to determine the fraction of binaries among the multiple stellar populations within each pair of simulated diagrams. For estimating the uncertainties associated with the observed fractions of 1P binaries, we assumed that the error corresponds to the root mean scatter of the 10,000 values of f_{bin}^{1P} derived from the simulated diagrams. We adopted a similar criterion to estimate the uncertainties associated with the best estimates of the fractions of 2P and mixed binaries.

3.2. The upper main sequence

To investigate the binaries among the bright MS stars ($17.25 < m_{F814W} < 19.10$ mag) we used the procedure described in Section 3.1 and by [Milone et al. \(2020\)](#). We took advantage of the $\Delta_{CF275W,F343N,F438W}$ vs. $\Delta_{F275W,F814W}$ ChM derived by [Milone & Marino \(2022\)](#) and reproduced in the left panels of Figure 5 to identify the probable 1P (crimson points in the bottom-left panel of Figure 5) and 2P stars. In addition, we selected by eye four groups of 2P stars, namely $2P_\alpha$, $2P_\beta$, $2P_\gamma$, $2P_\delta$, and $2P_\epsilon$ that we colored pink, orange, aqua, cyan, and blue, respectively.

We used the same colors to represent the selected stars in the m_{F814W} vs. $C_{F275W,F343N,F438W}$ pseudo-CMD plotted in the right panel of Figure 5. As shown in the inset, the selected stellar groups define distinct fiducial lines.

On the contrary, we verified that the fiducials of 1P and 2P stars of 47 Tucanae are nearly coincident in the m_{F814W}

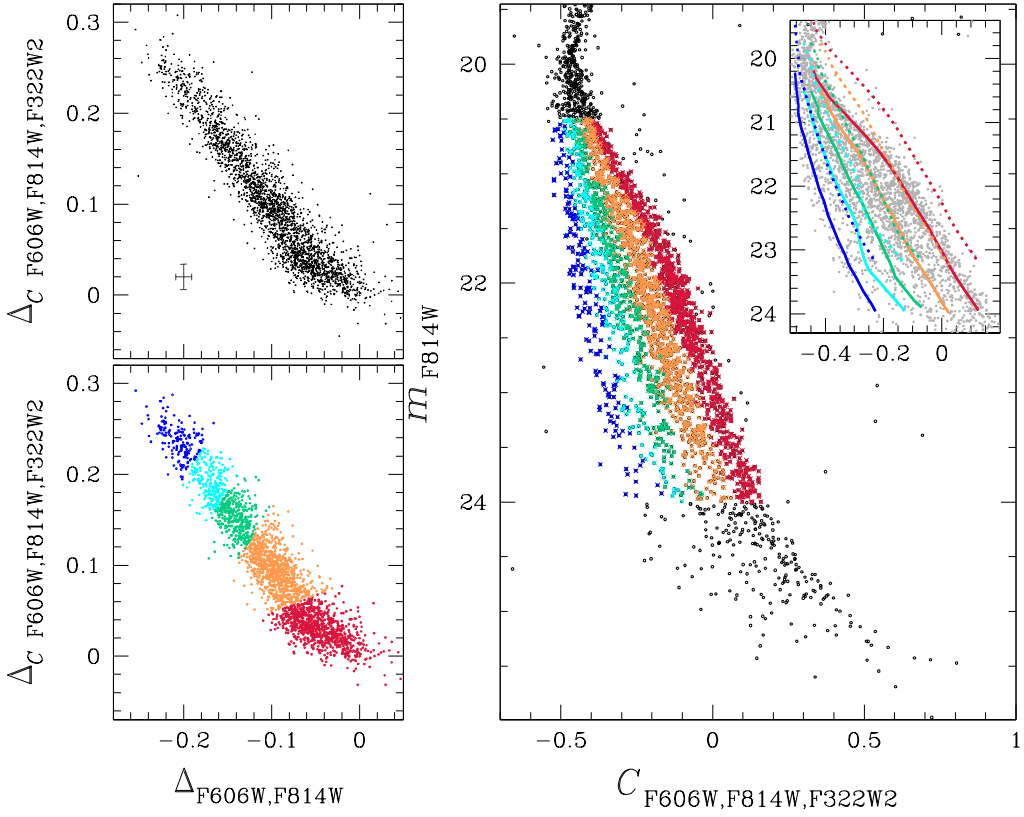


Fig. 1. $\Delta_{C_{F606W,F814W,F322W2}}$ vs. $\Delta_{F606W,F814W}$ ChMs for M-dwarfs with $20.5 < m_{F814W} < 24.00$ mag (left panels) and m_{F814W} vs. $C_{F606W,F814W,F322W2}$ pseudo-CMD of M-dwarfs from Marino et al. (2024a) (right panel). The probable 1P, 2P_A, 2P_B, 2P_C, and 2P_D stars, selected from the ChM, are colored crimson, orange, green, cyan, and blue, respectively. The inset in the right panel is a zoom of the m_{F814W} vs. $C_{F606W,F814W,F322W2}$ pseudo-CMD around the MS region where the five stellar populations are more-clearly distinguishable. The fiducial lines of the five stellar populations are represented with continuous colored lines, while the dotted lines represent the corresponding fiducial lines for equal-luminosity binaries.

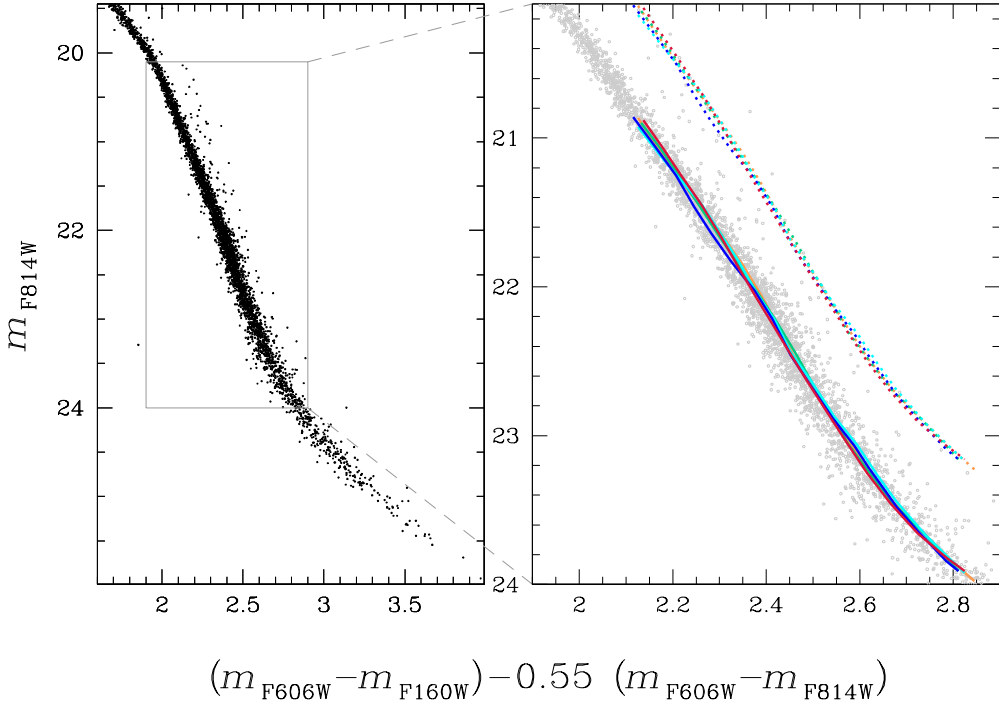


Fig. 2. *Left.* m_{F814W} as a function of the color difference $(m_{F606W} - m_{F160W}) - 0.55(m_{F606W} - m_{F814W})$ for the stars plotted in Figure 1. *Right.* Zoom in of the pseudo-CMD plotted in the left panel around the MS region used to derive the ChM. The continuous colored lines, which are partially overlapped with each other, are the fiducial lines of the five populations identified in the ChM of Figure 1. The fiducials of the corresponding sequences of equal-luminosity binaries are represented with dotted lines.

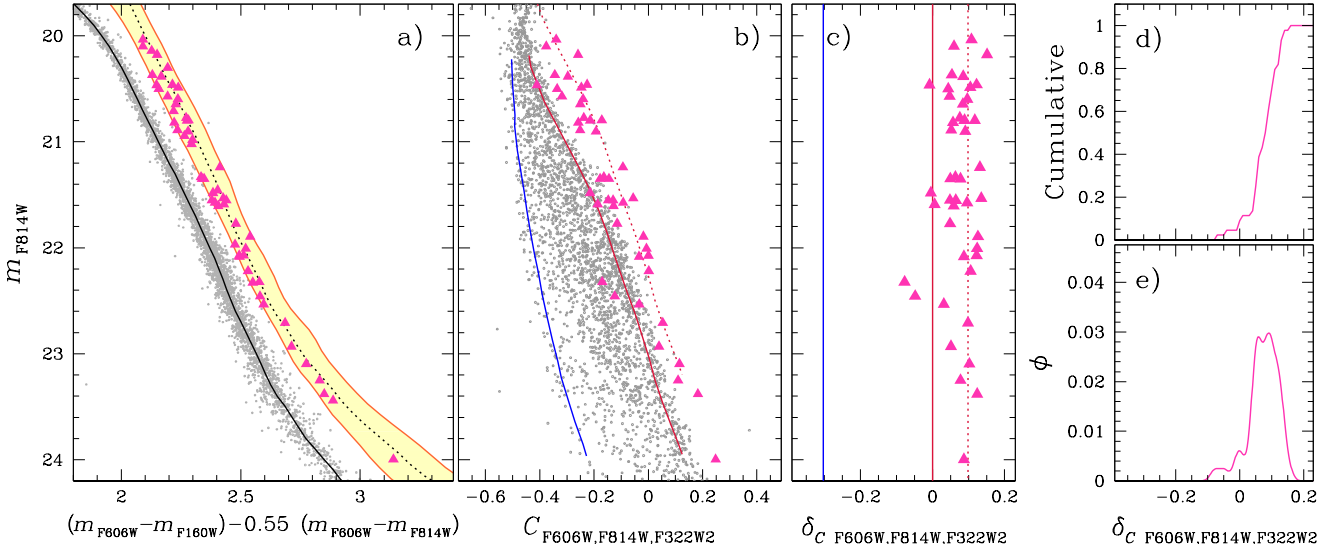


Fig. 3. Reproduction of the m_{F814W} vs. $(m_{\text{F606W}} - m_{\text{F160W}}) - 0.55(m_{\text{F606W}} - m_{\text{F814W}})$ pseudo-CMD of Figure 2 (panel a). The MS fiducial is represented with the continuous black line, whereas the dotted line is the fiducial of equal-luminosity binaries. The orange lines mark the boundaries of the yellow shaded region that we used to select the binaries (magenta triangles). Panel b shows the m_{F814W} vs. $C_{\text{F606W},\text{F814W},\text{F322W}2}$ pseudo-CMD. The fiducials of 1P and 2P_D stars are represented with continuous red and blue lines, respectively, and the equal-luminosity 1P binaries fiducial is indicated by the red dotted line. The verticalized m_{F814W} vs. $\delta_{\text{CF606W},\text{F814W},\text{F322W}2}$ diagram is plotted in panel c, while the $\delta_{\text{CF606W},\text{F814W},\text{F322W}2}$ cumulative and kernel-density distributions are plotted in panels d and e, respectively.

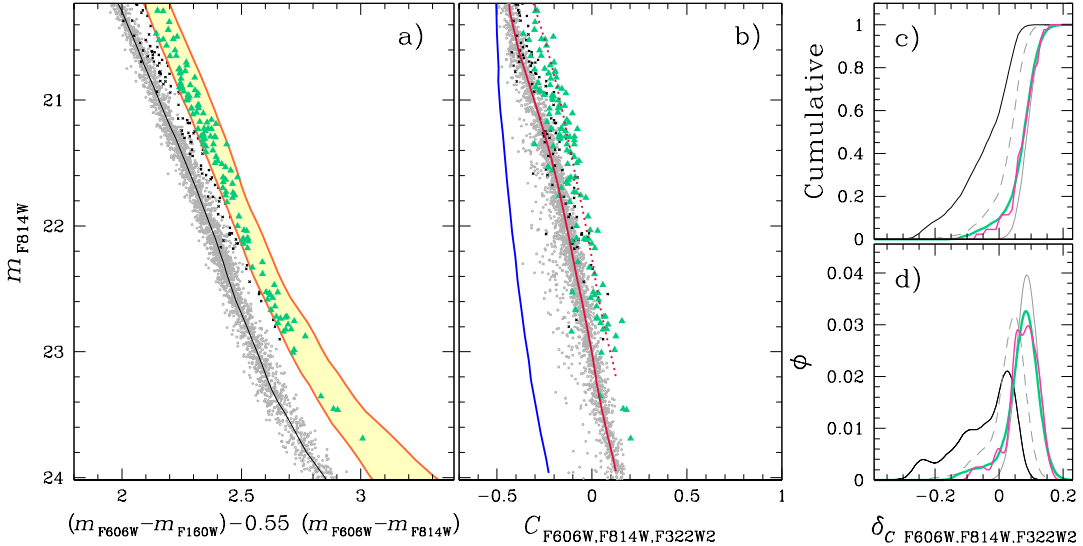


Fig. 4. Simulated m_{F814W} vs. $(m_{\text{F606W}} - m_{\text{F160W}}) - 0.55(m_{\text{F606W}} - m_{\text{F814W}})$ (panel a) and m_{F814W} vs. $C_{\text{F606W},\text{F814W},\text{F322W}2}$ (panel b) pseudo-CMDs. The adopted fractions of 1P, 2P, and mixed binaries provide the best fit with the observations. The selected binaries, which are located within the yellow shaded area of the panel-a diagram, are marked with aqua triangles, whereas the remaining binaries are represented with black symbols. For clarity, the number of plotted simulated binaries is three times larger than the number of observed binaries. The lines plotted in panels a and b reproduce the fiducial lines that we defined in Figure 3. Panels c and d compare the $\delta_{\text{CF606W},\text{F814W},\text{F322W}2}$ cumulative and the kernel density distributions, respectively, for the observed binaries (magenta lines) and the best-fit simulations (aqua lines). For completeness, we show the distributions of 1P binaries (gray continuous lines), 2P binaries (black continuous lines), and mixed binaries (gray dashed lines).

vs. $(m_{\text{F336W}} - m_{\text{F814W}}) - 0.40(m_{\text{F606W}} - m_{\text{F814W}})$ pseudo-CMD (panel a of Figure 6). Hence, we used this diagram to identify the sample of 57 probable binaries along the MS. The selected binaries are represented with magenta triangles and are located within the yellow-shaded region of the pseudo-CMD of Figure 6a. The latter is defined as in Figure 3a. In this case, the blue bound-

ary corresponds to the fiducial of MS binaries with a F814W luminosity difference of 1.6 mag.

We used the fiducial lines of 2P_D, 1P stars, and equal-luminosity 1P binaries superimposed on the m_{F814W} vs. $C_{\text{F275W},\text{F336W},\text{F438W}}$ pseudo-CMD of Figure 6b to derive the verticalized m_{F814W} vs. $\delta_{\text{CF275W},\text{F343N},\text{F438W}}$ diagram plotted in Figure 6c. To do that, we used the Equations 3 and assumed that

Field	radius [arcmin]	m_{F814W} interval [mag]	$f_{\text{bin}}^{\text{IP}}$	$f_{\text{bin}}^{\text{MIX}}$	$f_{\text{bin}}^{\text{2P}}$
External	5.38-7.95	20.25-24.00	84.8±5.0%	7.0±4.5%	8.2±4.5%
Central	0.77-1.73	17.25-19.10	17.3±7.3%	26.8±7.3%	55.8±8.0%
Central	0.77-2.26	17.25-17.80	25.6±9.5%	20.9±8.3%	53.5±10.5%
External	5.09-7.36	17.25-17.80	100±6.5%	0.0±6.5%	0.0±6.5%

Table 2. This table provides, for each dataset in the central and external fields, the studied radial and m_{F814W} magnitude intervals, and the fractions of 1P, mixed, and 2P binaries.

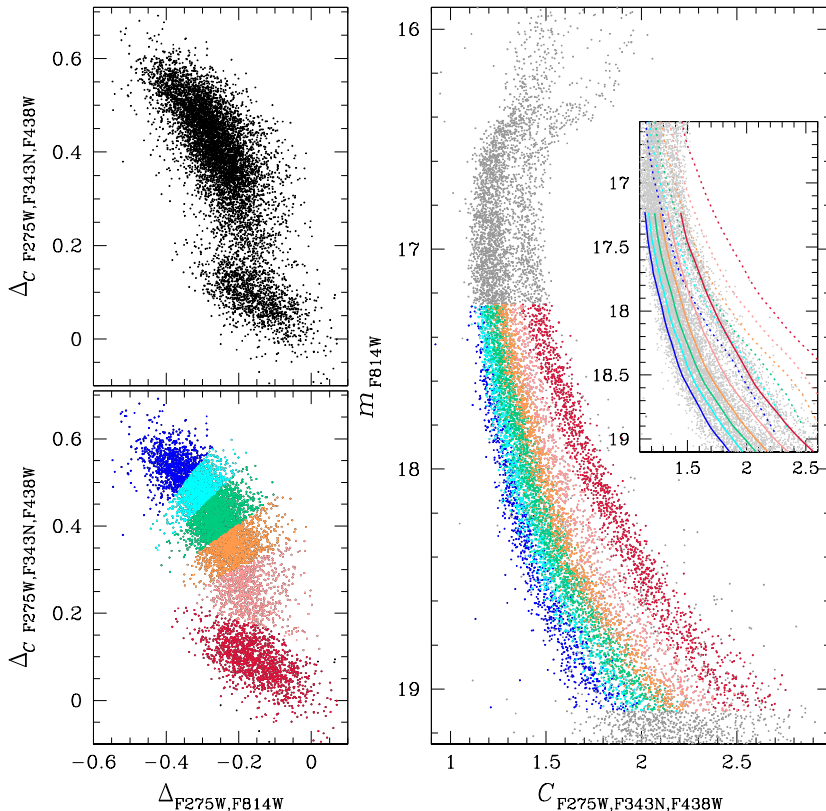


Fig. 5. $\Delta_{\text{CF275W},\text{F343N},\text{F438W}}$ vs. $\Delta_{\text{F275W},\text{F814W}}$ ChMs for MS stars with $17.25 < m_{\text{F814W}} < 19.10$ mag (left panels) and m_{F814W} vs. $C_{\text{F275W},\text{F343N},\text{F438W}}$ pseudo-CMD (right panel) of stars in the central field from Milone & Marino (2022). The probable 1P stars are colored crimson, whereas the five groups of 2P stars, namely α , β , γ , δ , and ϵ that we selected from the ChM are colored pink, orange, aqua, cyan, and blue, respectively. The continuous lines superimposed on the diagram in the inset of the right panel represent the fiducial lines of the six stellar populations, while the corresponding fiducial lines of equal-luminosity binaries are represented with dotted lines.

W_1 and W_{II} correspond to the $C_{\text{F275W},\text{F336W},\text{F438W}}$ pseudo-color distance between the continuous blue and red fiducials and between the continuous red and dotted red fiducials, respectively, at $m_{\text{F814W}} = 18.3$ mag. The cumulative and the kernel-density distributions of the selected binaries are represented in panels d and e of Figure 6.

3.3. The radial distribution of 1P and 2P binaries

The analysis presented in the previous subsections reveals a predominance of 1P binaries in the outer field, whereas the central field hosts significant amounts of 1P, 2P, and mixed binaries. However, the results in the central field are based on bright MS stars, whereas the study of the outer field is focused on M-dwarfs.

To ensure that the results on radial distribution are not influenced by stellar mass and to disentangle the effects of stellar mass and radial distance on the frequencies of binaries among multiple stellar populations, we used the photometry in the F336W, F435W, F606W, and F814W bands, which is available for bright MS stars in both the central and the outer field. The procedure that we used to study the binaries among 1P and 2P stars is similar to the one presented in Section 3.2 and is illustrated in the Figures 7 and 8 for stars in the central and external field, respectively. Similarly to what we have done in Section 3.2, we used the m_{F814W}

To derive the fractions of 1P, 2P, and mixed binaries, we used the procedure outlined in Section 3.1 and compared the observed $\delta_{\text{CF275W},\text{F343N},\text{F438W}}$ cumulative distributions and the cumulative distributions of grids of simulated binaries. The best match is provided by a fraction of $17.3\pm7.3\%$ 1P binaries, $55.8\pm8.0\%$ 2P binaries, and $26.8\pm7.3\%$ mixed binaries.

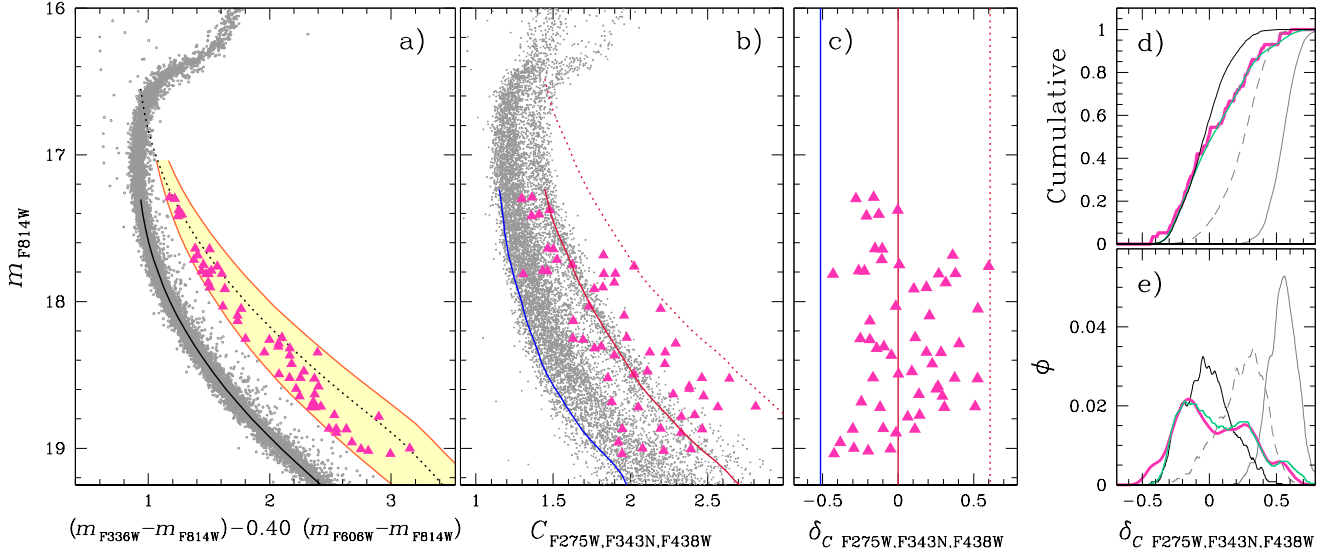


Fig. 6. m_{F814W} vs. $(m_{\text{F336W}} - m_{\text{F814W}}) - 0.40(m_{\text{F606W}} - m_{\text{F814W}})$ (panel a) and m_{F814W} vs. $C_{\text{F275W},\text{F343N},\text{F438W}}$ (panel b) pseudo-CMDs of stars in the central field. Panel c shows the verticalized m_{F814W} vs. $\delta_{C_{\text{F275W},\text{F336W},\text{F435W}}}$ diagram for the MS-MS binaries that we selected in panel a and represented with magenta triangles in panels a, b, and c. The $\delta_{C_{\text{F275W},\text{F336W},\text{F435W}}}$ cumulative and the kernel-density distributions of the studied binaries are illustrated with magenta lines in panels d and e, respectively, whereas the corresponding distributions for the simulated binaries that provide the best-fit with the observations are colored aqua. The gray and black lines correspond to the cumulative and the kernel-density distributions of 1P and 2P binaries alone, while the gray dashed lines represent the same distributions for mixed binaries. The continuous and the dotted black line plotted in panel a is the MS fiducial line and the fiducial of equal-luminosity binaries, whereas the orange lines delimit the yellow-shaded area of the CMD, which hosts the studied binaries. The blue lines plotted in panels b and c correspond to the fiducials of $2P_\delta$ stars, whereas the red-continuous and red-dotted lines are the fiducial lines of 1P stars and the fiducial lines of equal-luminosity 1P binaries, respectively.

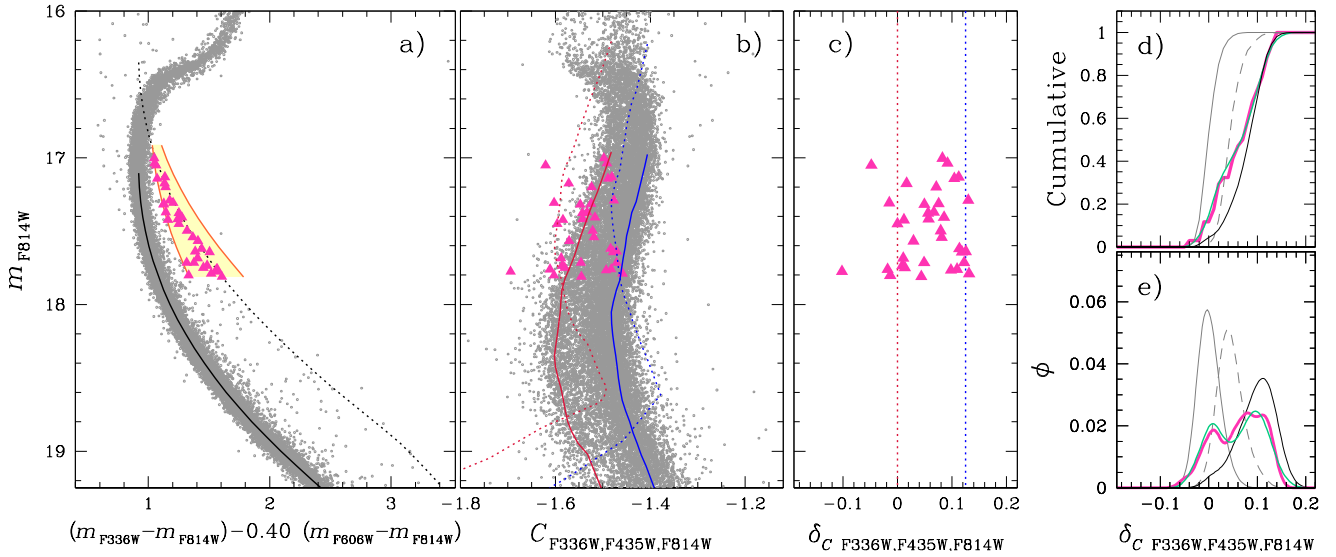


Fig. 7. Reproduction of the m_{F814W} vs. $(m_{\text{F336W}} - m_{\text{F814W}}) - 0.40(m_{\text{F606W}} - m_{\text{F814W}})$ pseudo-CMD of stars in the central field plotted in Figure 5 (panel a). Panel b shows the m_{F814W} vs. $C_{\text{F336W},\text{F435W},\text{F814W}}$ pseudo-CMDs, whereas the verticalized m_{F814W} vs. $\delta_{C_{\text{F336W},\text{F435W},\text{F814W}}}$ diagram for the MS-MS binaries is plotted in panel c. The binaries are selected in panel a and represented with magenta triangles in panels a, b, and c. The red and blue lines superimposed on the diagram plotted in panel b are the fiducials of 1P and $2P_\delta$ stars, respectively, while the corresponding fiducial lines of equal-luminosity binaries are represented with dotted lines in panels b and c. Panels d and e show the cumulative and kernel-density $\delta_{C_{\text{F336W},\text{F435W},\text{F814W}}}$ distributions, respectively, for the observed binaries (magenta continuous lines), for the simulated binaries that provide the best match with the observations (aqua continuous lines), 1P binaries (gray continuous lines), mixed binaries (gray dashed lines), and 2P binaries (black continuous lines).

vs. $(m_{\text{F336W}} - m_{\text{F814W}}) - 0.40(m_{\text{F606W}} - m_{\text{F814W}})$ pseudo-CMD to identify the candidate binaries. In this case, we selected all candidate binary systems where the F814W luminosity of the two

components differs by less than 1.8 mag (magenta triangles in Figures 7 and 8).

The b panels of these figures highlight the selected binaries in the m_{F814W} vs. $C_{\text{F336W},\text{F435W},\text{F814W}}$ pseudo-CMDs. These diagrams

provide a smaller pseudo-color separation between 1P and 2P stars (e.g. Jang et al. 2022; Milone & Marino 2022). Moreover, the fiducial lines of equal-luminosity 1P and 2P binaries cross their respective single-stars fiducial lines around $m_{\text{F814W}} = 17.8$ and 19.0 mag, thus making it challenging to identify binaries among multiple populations for $m_{\text{F814W}} \gtrsim 17.8$. Nevertheless, this diagram allows us to homogeneously analyse bright MS stars with different radial distances.

The c panels of Figures 7 and 8 show the m_{F814W} vs. $\Delta_{\text{CF336W},\text{F435W},\text{F814W}}$ diagram for the selected binaries. In this case, we used the fiducial lines of equal-luminosity binaries to verticalize the pseudo-CMD. Finally, panels d and e of Figures 7 and 8 illustrate the $\Delta_{\text{CF336W},\text{F435W},\text{F814W}}$ cumulative and kernel-density distributions (magenta lines) of the selected binaries. We also show the distributions of the simulated binaries that provide the best fit with the observations (aqua lines), and of 1P binaries (gray continuous lines), mixed binaries (gray dashed lines), and 2P binaries (black lines).

We found that the central field hosts both 1P, 2P, and mixed binary systems, which comprise $25.6 \pm 9.5\%$, $53.5 \pm 10.5\%$, and $20.9 \pm 8.3\%$ of the 35 studied binaries, respectively. In contrast, the six binary stars that we studied in the outer-field are all composed of 1P pairs. The results of this section thus confirm the radial trend in the fraction of 1P and 2P binaries found in the previous subsection using M-dwarfs for the outer field.

4. Chromosome map of binaries

In our opinion, the procedure introduced in the previous section is the optimal method for quantifying the fractions of binaries among 1P and 2P stars in GCs. Furthermore, the examination of the ChM can offer a qualitative yet direct perspective on the distribution of binaries among the different populations.

The top panel of Figure 9 shows the simulated $\Delta_{\text{CF275W},\text{F343N},\text{F435W}}$ vs. $\Delta_{\text{F275W},\text{F814W}}$ ChM for MS binaries of 47 Tucanae with $17.25 < m_{\text{F814W}} < 19.10$ mag. Specifically, the crimson, orange, and teal colors correspond to 1P, $2P_\beta$, and $2P_\epsilon$ binaries, respectively.

The ordinate of this diagram is derived as in Milone et al. (2017) by using the m_{F814W} vs. $C_{\text{F275W},\text{F343N},\text{F438W}}$ diagram. The abscissa is obtained from the m_{F814W} vs. $m_{\text{F275W}} - m_{\text{F814W}}$ CMD and is calculated as:

$$\Delta_{\text{F275W},\text{F814W}}^{\text{bin}} = \begin{cases} \Delta_{\text{F275W},\text{F814W}}, & \text{for } \Delta_{\text{F275W},\text{F814W}} \leq 0, \\ W_{\text{bin}} \left(1 + \frac{X - X_{\text{fiducial bin}}}{X_{\text{fiducial bin}} - X_{\text{fiducial R}}} \right), & \text{for } \Delta_{\text{F275W},\text{F814W}} > 0 \end{cases} \quad (2)$$

where the quantity $\Delta_{\text{F275W},\text{F814W}}$ is defined by Milone et al. (2017, see their section 3.2) and W_{bin} is the $m_{\text{F275W}} - m_{\text{F814W}}$ color separation at $m_{\text{F814W}} = 18.3$ mag between the fiducial line that marks the red boundary of the MS (fiducial R) and the corresponding fiducial line shifted by 0.752 mag to the bright side (fiducial bin, see Milone et al. 2017, for details). To simulate the binary systems, we combined the colors and the magnitudes of MS stars located on the fiducial lines of each population. Stellar masses were inferred using the isochrones from Dotter et al. (2008), which provide the best match with the m_{F814W} vs. $m_{\text{F606W}} - m_{\text{F814W}}$ CMD. For the binaries, we adopted a flat mass-ratio distribution. We used the same method to generate $\Delta_{\text{CF336W},\text{F435W},\text{F814W}}$ vs. $\Delta_{\text{F435W},\text{F814W}}^{\text{bin}}$ and $\Delta_{\text{CF606W},\text{F814W},\text{F322W2}}$ vs. $\Delta_{\text{F606W},\text{F814W}}^{\text{bin}}$ ChMs that we plotted in the middle and bottom panel of Figure 9 for MS binaries in the same magnitude intervals used for real stars. Clearly, the 1P and 2P binaries populate different regions of these ChMs.

The ChMs of the observed 47 Tucanae stars are shown in Figure 10, where we also plot with pink colors the simulated 1P binaries. The binary systems studied in Section 3 are marked with magenta triangles, whereas the remaining probable binaries are represented with black circles. The simulated 1P binaries overlap with a small portion of the observed binaries in the central-field ChMs, whereas the majority of both observed and simulated binaries are located in the same region of the outer-field ChM. These observations qualitatively confirm the conclusion of Section 3 that the central field is populated by both 1P and 2P binaries, whereas 1P binaries are more prevalent in the external regions of 47 Tucanae.

4.1. Binaries and multiple populations along the RGB

For completeness, in this subsection we investigate the frequency of 1P and 2P binaries along the RGB. To investigate the distribution of binary systems composed of at least one RGB star in the m_{F814W} vs. $m_{\text{F275W}} - m_{\text{F814W}}$ CMD, we show the fiducial line of MS, SGB, and RGB stars (solid aqua line in the left panel of Figure 11) and the fiducial of binary systems composed of pairs of stars with the same luminosity and evolutionary stage (aqua dashed line). We also plot with a dot-dashed line the fiducial line of binaries where one of the two components is located on the MS turn off. The binary systems fainter than $m_{\text{F814W}} \sim 13.8$ mag and composed of RGB and MS stars, RGB and SGB stars, or by pairs of RGB stars populated the CMD region limited by the continuous line and the dot-dashed line. In the case of binaries with $m_{\text{F814W}} \lesssim 13.8$ mag the blue boundary is the dashed line⁵. This region of the CMD is also populated by evolved blue stragglers.

The middle panel of Figure 11 shows the m_{F814W} vs. $C_{\text{F275W},\text{F343N},\text{F435W}}$ pseudo-CMD of the stars in the central field. The crimson fiducials refer to single 1P stars (solid line), to binaries composed of 1P stars with the same luminosity (dashed line) and binary systems composed of a 1P star located on the MS turn off with a 1P companion (dot-dashed lines). All 1P RGB binaries are located in the area encompassed by these lines.

The $\Delta_{\text{F275W},\text{F343N},\text{F435W}}$ vs. $\Delta_{\text{F275W},\text{F814W}}^{\text{bin}}$ ChM is plotted in the top-right panel for RGB stars with $13.0 < m_{\text{F814W}} < 16.0$ mag. This ChM is derived by following the recipe used for the MS but in this case we account for the fact that the fiducial of equal-luminosity RGB binaries is bluer than the RGB boundaries, by using the relation:

$$\Delta_{\text{F275W},\text{F814W}}^{\text{bin}} = \begin{cases} \Delta_{\text{F275W},\text{F814W}}, & \text{for } \Delta_{\text{F275W},\text{F814W}} \geq -W, \\ W_{\text{bin}} \left(\frac{X - X_{\text{fiducial B}}}{X_{\text{fiducial B}} - X_{\text{fiducial bin}}} \right) - W, & \text{for } \Delta_{\text{F275W},\text{F814W}} < -W \end{cases} \quad (3)$$

where the F275W–F814W RGB width, W , and the quantity $\Delta_{\text{F275W},\text{F814W}}$ is defined by Milone et al. (2017, see their sections 3.1 and 3.2), and W_{bin} is the $m_{\text{F275W}} - m_{\text{F814W}}$ absolute value of the color separation at $m_{\text{F814W}} = 14.8$ mag between the fiducial line that marks the blue boundary of the MS (fiducial B) and the corresponding fiducial line shifted by 0.752 mag to the bright side (fiducial bin).

⁵ The fiducial lines shown in the left panel of Figure 11 are used to illustrate the CMD region populated by RGB binaries. For simplicity, we derived these fiducials by considering both 1P and 2P stars. The fiducial of single RGB stars composed by 1P stars only and the fiducials of binary systems that host one 1P RGB star would exhibit slightly redder $m_{\text{F275W}} - m_{\text{F814W}}$ colors. Similarly, the corresponding fiducials derived from 2P RGB stars would be bluer than those plotted in Figure 11.

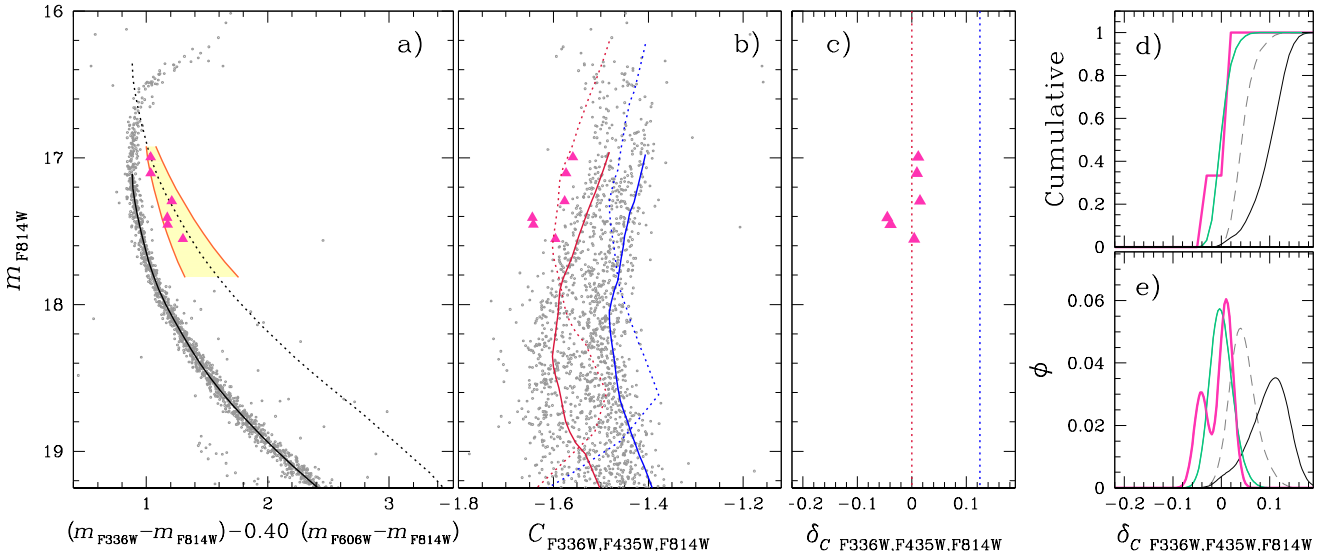


Fig. 8. Same as in Figure 7 but for stars in the outer field.

As demonstrated by [Marino et al. \(2019\)](#), RGB binaries exhibit lower values of $\Delta_{F275W,F814W}$ than the bulk of single stars, thus populating the left region of the ChM. We have used magenta triangles to select a sample of 19 probable binaries in the ChM and used the same symbols to represent them in the other panels of Figure 11. As expected, the selected stars populate the region of the m_{F814W} vs. $m_{F275W} - m_{F814W}$ CMD occupied by binaries.

To qualitatively associate binary stars with 1P and 2P stars, we simulated RGB binaries composed of 1P RGB stars, and 2P RGB stars with intermediate and extreme chemical compositions. The simulated binaries are represented with crimson, orange, and teal colors, respectively, in the ChM plotted in the bottom-right panel of Figure 11 and are superimposed on the observed RGB stars (gray points). We notice that half a dozen binaries only are consistent with 1P binaries, whereas the remaining selected binaries are probably composed of 2P stars or mixed. A similar conclusion is provided by the visual inspection of the m_{F814W} vs. $C_{F275W,F343N,F435W}$ pseudo-CMD plotted in the middle panel of Figure 11. A quantitative determination of the frequency of binaries among 1P and 2P RGB stars is challenged by the fact that the selected candidate binaries could comprise evolved blue stragglers, for which accurate models are not available to us. Nevertheless, the comparison between the observed ChM of RGB stars in 47 Tucanae and the simulated ChMs of 1P and 2P binaries corroborates the conclusion derived from MS stars that both 1P and 2P binaries populate the central region of 47 Tucanae.

5. Summary and discussion

In this paper, we used multi-band *HST* and *JWST* photometry of 47 Tucanae to estimate the fraction of binaries among 1P and 2P stars. In contrast with the previous works on other GCs, which are limited either to the cluster center or the external regions ([D’Orazi et al. 2010](#); [Lucatello et al. 2015](#); [Dalessandro et al. 2018](#); [Marino et al. 2019](#); [Kamann et al. 2020](#); [Milone et al. 2020](#)), we homogeneously analysed two distinct fields with different radial distances from the center of 47 Tucanae.

We used the method by [Milone et al. \(2020\)](#), which consists of three main steps, including i) the identification of 1P and 2P stars, ii) the selection of binary systems composed of stars with similar

luminosities, and iii) the analysis of pseudo-colors of the selected binaries, which are indicative of their chemical composition.

In the central field, we took advantage of the $\Delta_{CF275W,F343N,F435W}$ vs. $\Delta_{F275W,F814W}$ ChM to identify the bulk of 1P and 2P stars along the upper MS, together with five sub-groups of $2P_{\alpha-\epsilon}$ stars. We identified a sample of MS-MS binaries by using the pseudo-CMD m_{F814W} vs. $(m_{F336W} - m_{F814W}) - 0.40(m_{F606W} - m_{F814W})$, where the fiducial lines of the multiple stellar populations are nearly coincident. Finally, we analyzed the $C_{F275W,F343N,F435W}$ pseudo-color distribution of the observed binary stars and compared it to the distributions from a large set of simulated stellar populations. These simulations encompassed various combinations of 1P, 2P, and mixed stars. We find that about 18% and 56% of the studied binaries are composed of 1P and 2P stars, respectively. The remaining $\sim 26\%$ of binaries are probable mixed stellar systems.

In the external field, we analyzed both M-dwarf stars. The 1P and 2P stars are identified from the $\Delta_{CF606W,F814W,F322W2}$ vs. $\Delta_{F606W,F814W}$ ChM, whereas the binaries are selected from the m_{F814W} vs. $(m_{F606W} - m_{F160W}) - 0.55(m_{F606W} - m_{F814W})$ pseudo CMD. In this case, the fraction of binaries among the multiple populations is inferred by comparing the $\Delta_{CF606W,F814W,F322W2}$ pseudo-color of the selected binaries with that of a large sample of simulated binaries. Most binaries, $\sim 85\%$, are composed of 1P stars. These results are illustrated in the top panel of Figure 12 and are confirmed by the analysis of bright MS stars in the m_{F814W} vs. $C_{F336W,F435W,F814W}$ pseudo-CMD in both the inner and outer fields.

As illustrated in the bottom panel of Figure 12, the multiple stellar populations of 47 Tucanae exhibit different radial distributions, with 2P stars being significantly more centrally concentrated than the 1P (e.g. [Milone et al. 2012b](#); [Cordero et al. 2014](#); [Dondoglio et al. 2021](#); [Lee 2022](#); [Mehta et al. 2025](#)). In particular, the fraction of 1P stars in the cluster center and in the external field studied in this paper is $\sim 20\%$ and 40% , respectively ([Milone et al. 2017](#); [Marino et al. 2024a](#)).

The incidence of 1P binaries can be estimated as the ratio between the fractions of 1P binaries and the fractions of 1P stars (from [Milone et al. 2012b](#); [Marino et al. 2024a](#)) and the analogous relation can be adopted for the incidence of 2P binaries.

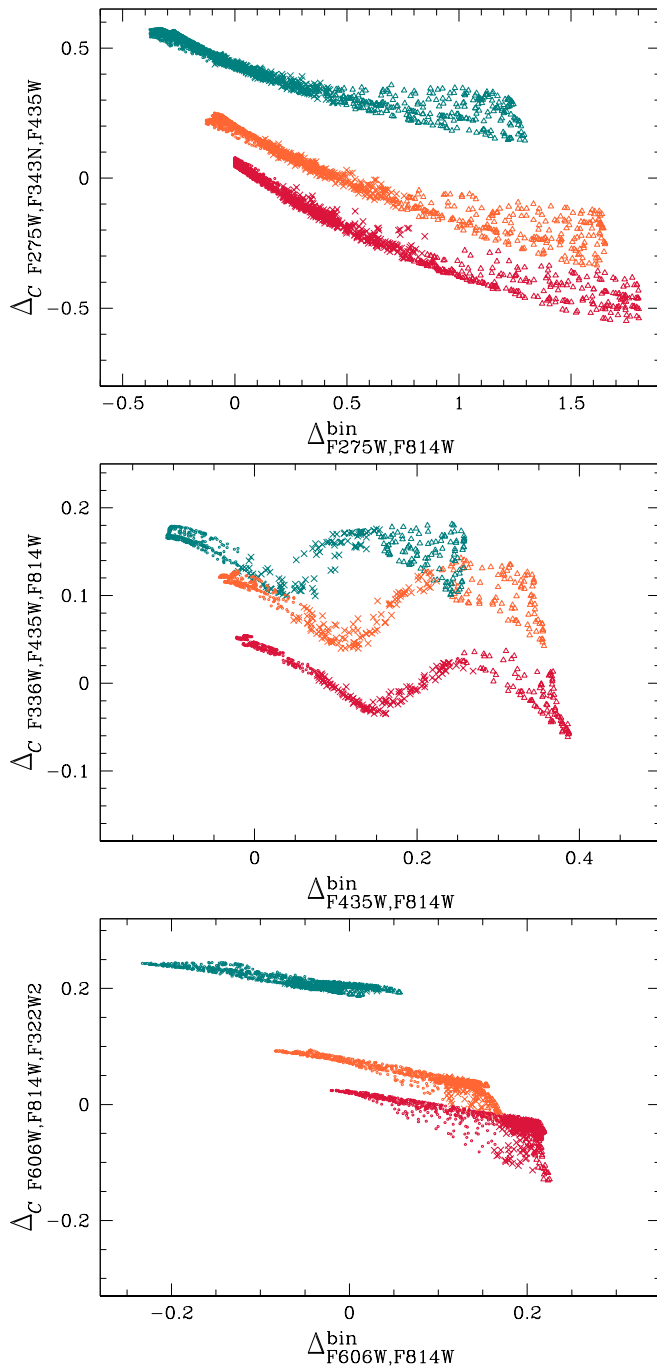


Fig. 9. Simulated ChMs for upper-MS stars of 47 Tucanae. Crimson, orange, and teal colors indicate 1P, 2P _{β} , and 2P _{ϵ} binaries, respectively. The triangles, crosses, and circles indicate the binaries with mass ratios $q > 0.8$, $0.6 < q < 0.8$, and $q < 0.6$, respectively.

Hence, in the cluster center, the incidence of 1P binaries is slightly (~ 1.3 times) higher than that of 2P binaries. In contrast, the outer regions predominantly feature 1P binaries.

The present-day fractions of binaries among 1P and 2P stars provide information on the origin and the dynamic evolution of multiple stellar populations in GCs. Binary systems have been widely investigated in the context of GC formation scenarios where the 2P stars formed in a high-density environment in the innermost region of a more-extended 1P. Such configuration is adopted in various scenarios for the formation of 2P stars (e.g. D'Ercole et al. 2008, 2012; Bekki 2010; Lacchin et al. 2022)

and consistent with the expected initial configuration of various scenarios (e.g. Bastian et al. 2013; Gieles et al. 2018).

Studies based on analytic calculations and N-body simulations suggest that the exact values of the current fractions of 1P and 2P binaries are influenced by several factors. These include the initial numbers and configurations of 1P and 2P stars, the evolution and disruption of binary systems, and the changes in the spatial distributions of 1P and 2P single and binary stars over time. Nevertheless, these simulations show that, due to the dense environment, 2P binaries evolve and are disrupted at a much higher rate than 1P binaries. Consequently, the present-day 2P population is expected to have a lower global binary incidence compared to the 1P population (Vesperini et al. 2011; Hong et al. 2015, 2016, 2019). These studies, which assume different initial radial distributions of 1P and 2P stars with the 2P initially more centrally concentrated, predict radial variations in the incidence of 1P and 2P binaries, with the most pronounced differences observed in the outermost regions of the cluster (e.g. Hong et al. 2016; Milone et al. 2020).

The evidence of a radial gradient in the incidence of 1P and 2P binaries in 47 Tucanae, and the fact that the external regions are mostly populated by 1P binaries are in general agreement with the predictions of those theoretical studies, and corroborate the possibility that 2P stars formed in a dense subsystem in the innermost cluster regions. Similarly, the finding of mixed binary systems composed of one 1P and one 2P star is qualitatively consistent with the findings of the simulations by Hong et al. (2015, 2016) who predicted that, due to stellar encounters, one of the binary-system components can be replaced by one of the interacting stars of a different population, thus producing a mixed binary system.

Acknowledgements. We thank the anonymous referee for their valuable suggestions, which have improved the manuscript. This work has been funded by the European Union – NextGenerationEU RRF M4C2 1.1 (PRIN 2022 2022MMEB9W: “Understanding the formation of globular clusters with their multiple stellar generations”, CUP C53D23001200006). (PI Anna F. Marino), from INAF Research GTO-Grant Normal RSN2-1.05.12.05.10 - (ref. Anna F. Marino) of the “Bando INAF per il Finanziamento della Ricerca Fondamentale 2022”, and from the European Union’s Horizon 2020 research and innovation programme under the Marie Skłodowska-Curie Grant Agreement No. 101034319 and from the European Union – NextGenerationEU (beneficiary: T. Ziliotto). SJ acknowledges support from the National Research Foundation of Korea (2022R1A2C3002992, 2022R1A6A1A03053472). J.-W. Lee acknowledges financial support from the Basic Science Research Program (grant No. 2019R1A2C2086290) through the National Research Foundation of Korea.

References

- Anderson, J. & King, I. R. 2006, PSFs, Photometry, and Astronomy for the ACS/WFC, Instrument Science Report ACS 2006-01, 34 pages
- Anderson, J., Sarajedini, A., Bedin, L. R., et al. 2008, AJ, 135, 2055
- Bastian, N., Lamers, H. J. G. L. M., de Mink, S. E., et al. 2013, MNRAS, 436, 2398
- Bastian, N. & Lardo, C. 2018, ARA&A, 56, 83
- Bekki, K. 2010, ApJ, 724, L99
- Bellini, A., Anderson, J., & Bedin, L. R. 2011, PASP, 123, 622
- Bellini, A. & Bedin, L. R. 2009, PASP, 121, 1419
- Bortolan, E., Bruce, J., Milone, A. P., et al. 2025, arXiv e-prints, arXiv:2503.09708
- Calura, F., D'Ercole, A., Vesperini, E., Vanzella, E., & Sollima, A. 2019, MNRAS, 489, 3269
- Cordero, M. J., Pilachowski, C. A., Johnson, C. I., et al. 2014, ApJ, 780, 94
- Cottrell, P. L. & Da Costa, G. S. 1981, ApJ, 245, L79
- Dalessandro, E., Mucciarelli, A., Bellazzini, M., et al. 2018, ApJ, 864, 33
- Dantona, F., Gratton, R., & Chieffi, A. 1983, Mem. Soc. Astron. Italiana, 54, 173
- D'Antona, F., Vesperini, E., Calura, F., et al. 2023, A&A, 680, L19
- D'Antona, F., Vesperini, E., D'Ercole, A., et al. 2016, MNRAS, 458, 2122
- de Mink, S. E., Pols, O. R., Langer, N., & Izzard, R. G. 2009, A&A, 507, L1
- Decressin, T., Meynet, G., Charbonnel, C., Prantzos, N., & Ekström, S. 2007, A&A, 464, 1029

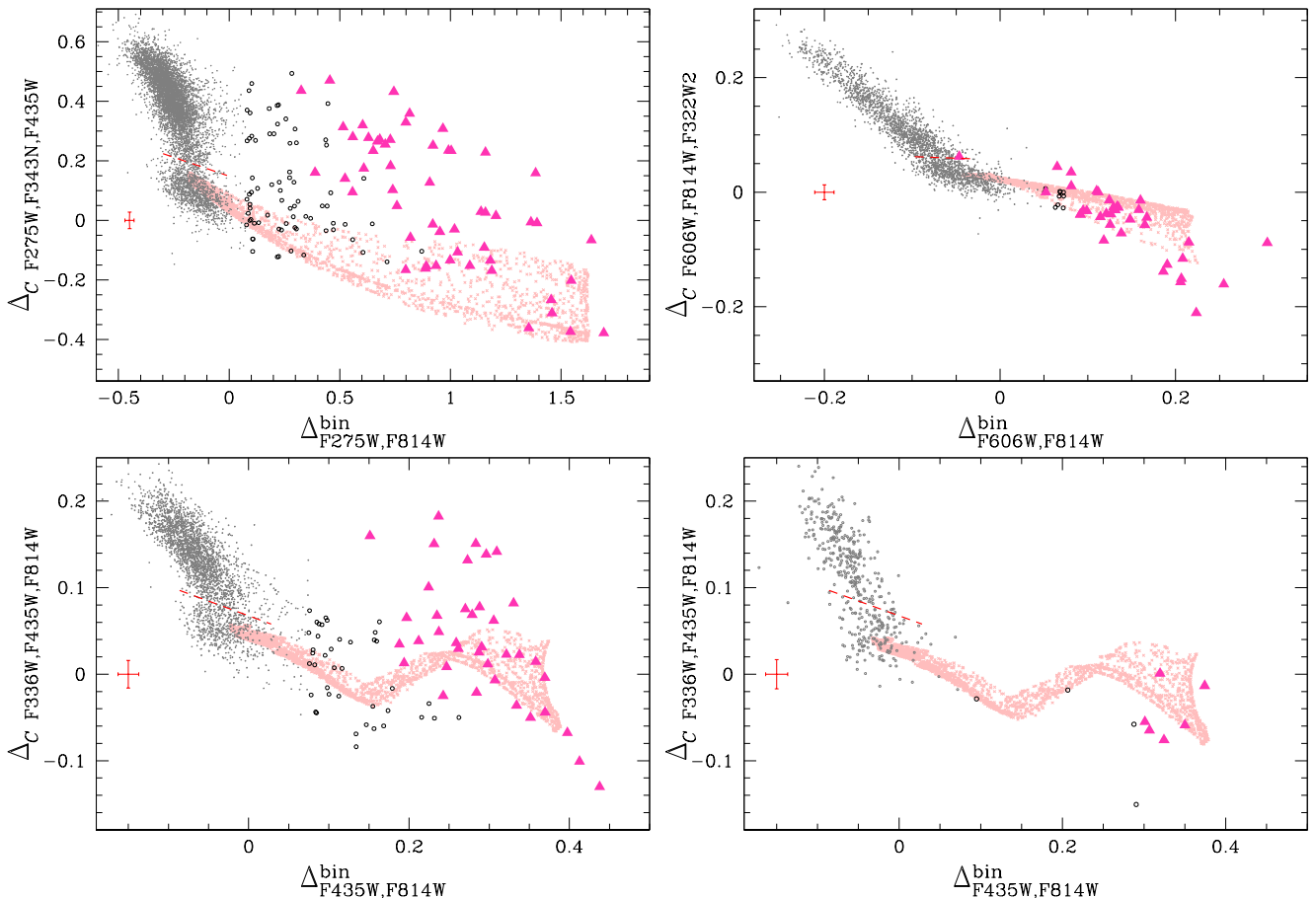


Fig. 10. ChMs for stars in the central field (left panels) and in the outer field (right panels). The binaries selected in Figures 3a, 6a, 7a, and 8a are represented with large magenta triangles. The remaining candidate binaries are plotted with black circles. The red-dashed lines separate the bulk of single 1P and 2P stars, which are located below and above the lines, respectively. The pink points show simulated 1P binaries.

- Denissenkov, P. A. & Hartwick, F. D. A. 2014, MNRAS, 437, L21
 D'Ercole, A., D'Antona, F., Carini, R., Vesperini, E., & Ventura, P. 2012, MNRAS, 423, 1521
 D'Ercole, A., Vesperini, E., D'Antona, F., McMillan, S. L. W., & Recchi, S. 2008, MNRAS, 391, 825
 Dondoglio, E., Milone, A. P., Lagioia, E. P., et al. 2021, ApJ, 906, 76
 D'Orazi, V., Gratton, R., Lucatello, S., et al. 2010, ApJ, 719, L213
 Dotter, A., Chaboyer, B., Jevremović, D., et al. 2008, ApJS, 178, 89
 Gieles, M., Charbonnel, C., Krause, M. G. H., et al. 2018, MNRAS, 478, 2461
 Gratton, R., Bragaglia, A., Carretta, E., et al. 2019, A&A Rev., 27, 8
 Gratton, R., Sneden, C., & Carretta, E. 2004, ARA&A, 42, 385
 Gratton, R. G., Carretta, E., & Bragaglia, A. 2012, A&A Rev., 20, 50
 Harris, W. E. 1996, AJ, 112, 1487
 Hong, J., Patel, S., Vesperini, E., Webb, J. J., & Dalessandro, E. 2019, MNRAS, 483, 2592
 Hong, J., Vesperini, E., Sollima, A., et al. 2015, MNRAS, 449, 629
 Hong, J., Vesperini, E., Sollima, A., et al. 2016, MNRAS, 457, 4507
 Hypki, A., Giersz, M., Hong, J., et al. 2022, MNRAS, 517, 4768
 Jang, S., Milone, A. P., Legnardi, M. V., et al. 2022, MNRAS, 517, 5687
 Kamann, S., Giesers, B., Bastian, N., et al. 2020, A&A, 635, A65
 Kraft, R. P. 1994, PASP, 106, 553
 Lacchin, E., Calura, F., Vesperini, E., & Mastrobuono-Battisti, A. 2022, MNRAS, 517, 1171
 Lacchin, E., Mastrobuono-Battisti, A., Calura, F., et al. 2024, A&A, 681, A45
 Lee, J.-W. 2022, ApJS, 263, 20
 Lucatello, S., Sollima, A., Gratton, R., et al. 2015, A&A, 584, A52
 Luck, R. E. & Bond, H. E. 1991, ApJS, 77, 515
 Marino, A. F., Milone, A. P., Legnardi, M. V., et al. 2024a, ApJ, 965, 189
 Marino, A. F., Milone, A. P., Renzini, A., et al. 2024b, ApJ, 969, L8
 Marino, A. F., Milone, A. P., Sills, A., et al. 2019, ApJ, 887, 91
 McClure, R. D. 1989, in IAU Colloq. 106: Evolution of Peculiar Red Giant Stars, ed. H. R. Johnson & B. Zuckerman, 196
 Mehta, V. J., Milone, A. P., Casagrande, L., et al. 2025, MNRAS, 536, 1077
 Milone, A. P., Cordoni, G., Marino, A. F., et al. 2025, arXiv e-prints, arXiv:2501.08135
 Milone, A. P., Cordoni, G., Marino, A. F., et al. 2023a, A&A, 672, A161
 Milone, A. P. & Marino, A. F. 2022, Universe, 8, 359
 Milone, A. P., Marino, A. F., Dotter, A., et al. 2023b, MNRAS, 522, 2429
 Milone, A. P., Piotto, G., Bedin, L. R., et al. 2012a, A&A, 540, A16
 Milone, A. P., Piotto, G., Bedin, L. R., et al. 2012b, ApJ, 744, 58
 Milone, A. P., Piotto, G., Renzini, A., et al. 2017, MNRAS, 464, 3636
 Milone, A. P., Vesperini, E., Marino, A. F., et al. 2020, MNRAS, 492, 5457
 Muratore, F., Milone, A. P., D'Antona, F., et al. 2024, A&A, 692, A135
 Renzini, A. 2017, MNRAS, 469, L63
 Renzini, A., D'Antona, F., Cassisi, S., et al. 2015, MNRAS, 454, 4197
 Renzini, A., Marino, A. F., & Milone, A. P. 2022, MNRAS, 513, 2111
 Ventura, P., D'Antona, F., Mazzitelli, I., & Gratton, R. 2001, ApJ, 550, L65
 Vesperini, E., McMillan, S. L. W., D'Antona, F., & D'Ercole, A. 2011, MNRAS, 416, 355
 Wang, L., Kroupa, P., Takahashi, K., & Jerabkova, T. 2020, MNRAS, 491, 440

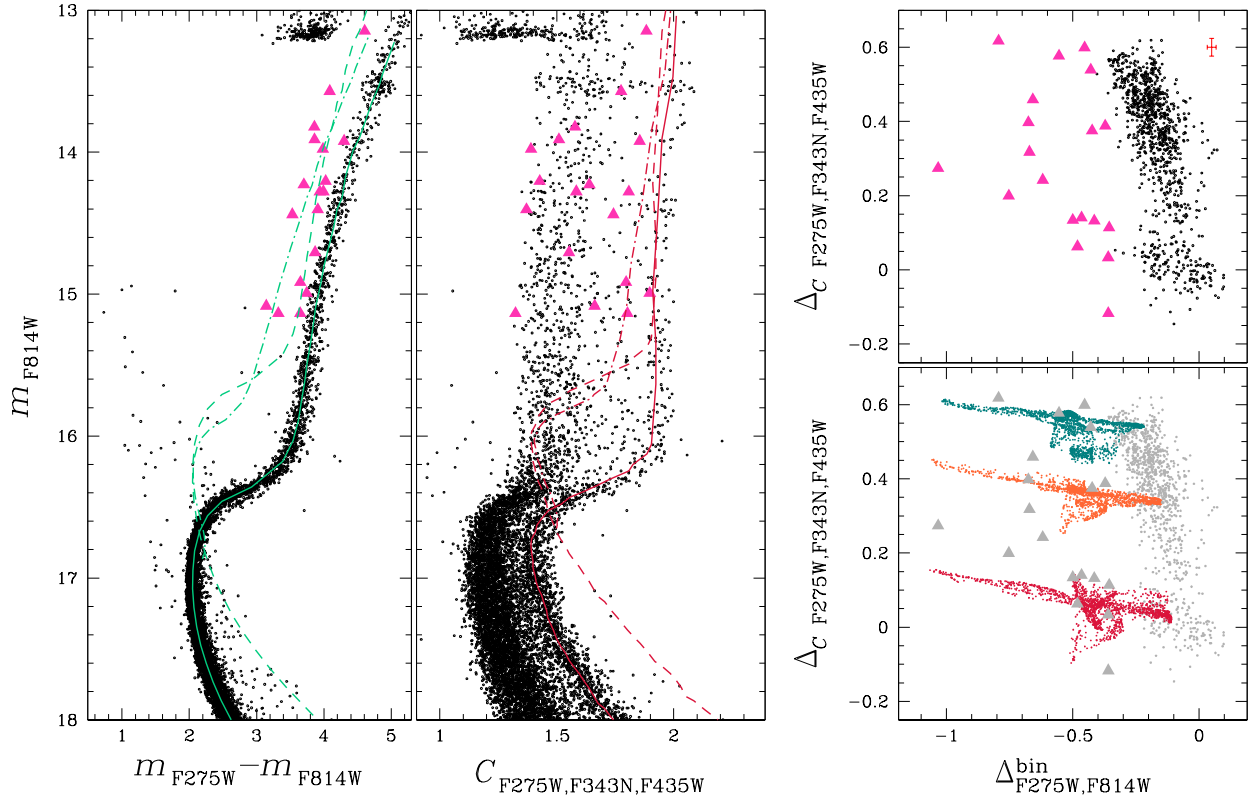


Fig. 11. m_{F814W} vs. $m_{\text{F275W}} - m_{\text{F814W}}$ CMD (left) and m_{F814W} vs. $C_{\text{F275W},\text{F343N},\text{F435W}}$ pseudo-CMD (middle) of stars in the central field zoomed in around the RGB. The solid aqua line plotted in the left-panel CMD is the fiducial line of the MS, SGB, and RGB. The dashed line represents the fiducial line of equal-luminosity stars, whereas the fiducial line of binary systems composed of one MS turn off star is plotted with the dot-dashed line. The probable RGB binaries, selected from the $\Delta_{\text{F275W},\text{F343N},\text{F435W}}$ vs. $\Delta_{\text{F275W},\text{F814W}}^{\text{bin}}$ ChM shown in the top-right panel, are represented with magenta gray triangles. The bottom-right panel illustrates the simulated ChM for RGB binaries composed of 1P stars (crimson) and 2P stars with intermediate (orange) and extreme (teal) chemical compositions. The gray points reproduce the observed ChM plotted in the top-right panel.

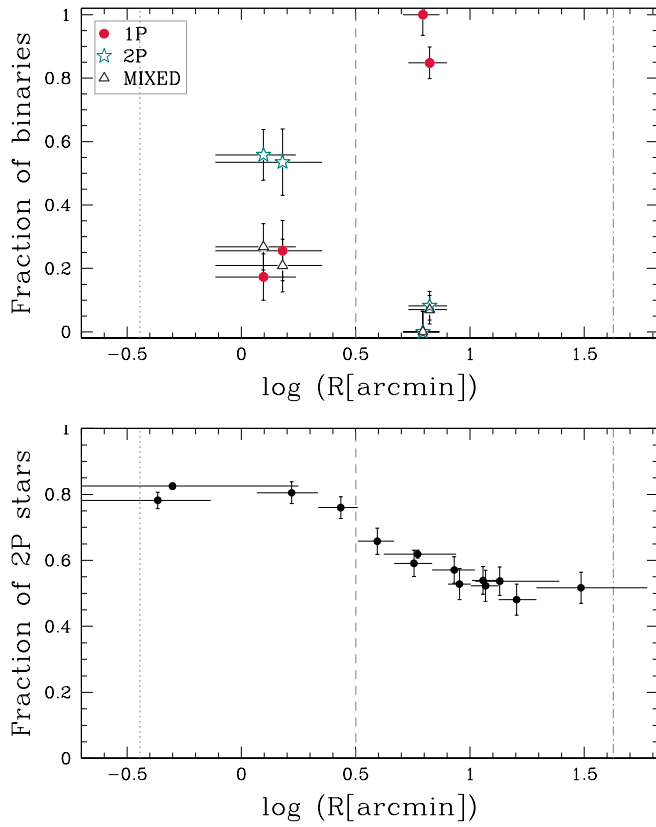


Fig. 12. *Top.* Fractions of 1P binaries (dots), 2P binaries (starred symbols), and mixed binaries (triangles) derived in this paper against the logarithm of the radial distance from the center of 47 Tucanae. *Bottom.* Fraction of 2P stars as a function of radial distance, in logarithm scale, from literature works (Milone et al. 2017; Dondoglio et al. 2021; Marino et al. 2024a; Mehta et al. 2025). The vertical dotted, dashed, and dashed-dotted lines mark the core, half-light, and tidal radius, respectively, from the 2010 edition of the Harris (1996) catalog.